Journal Pre-proof

Deep inside the colour: how optical microscopy contributes to the elemental characterization of a painting.

Anna Galli , M. Caccia , L. Bonizzoni , M. Gargano , N. Ludwig , G. Poldi , M. Martini

Please cite this article as: Anna Galli , M. Caccia , L. Bonizzoni , M. Gargano , N. Ludwig , G. Poldi , M. Martini , Deep inside the colour: how optical microscopy contributes to the elemental characterization of a painting., *Microchemical Journal* (2020), doi: https://doi.org/10.1016/j.microc.2020.104730

Highlights:

- The HSV model quantifies the visual perception of the hues of the flesh tones
- The descriptors analysis unveils non coincidental links between OM and XRF/FORS data
- OM reveals to be a plus to characterize the painting layers

Deep inside the colour: how optical microscopy contributes to the elemental characterization of a painting.

A. Galli[a,b], M. Caccia[b], L. Bonizzoni[c], M. Gargano[c], N. Ludwig[c], G. Poldi[d], M. Martini [b]

[a] CNR-IBFM, via F.lli Cervi 93, 20090 Segrate (IT)

[b] Dipartimento di Scienza dei Materiali, Università degli Studi di Milano-Bicocca, via R. Cozzi 55, 20125 Milano (IT) and INFN, Sezione Milano-Bicocca

[c] Dipartimento di Fisica "Aldo Pontemoli", Università degli Studi di Milano, via Celoria 16, 20161 Milano (IT)

[d] Centro Arti Visive (CAV), Università degli Studi di Bergamo, Via Pignolo 123, 24121 Bergamo (IT)

Corresponding author: Michele Caccia, Dipartimento di Scienza dei Materiali, Università degli Studi di Milano-Bicocca, via R. Cozzi 55, 20125 Milano (IT); email: michele.caccia@unimib.it

Abstract

In the context of paintings characterization, X-Ray Fluorescence (XRF) combined with Fibre Optics Reflectance Spectroscopy (FORS) is a well-known methodology. The latter allows to classify the pigments constituting the external layers (few microns) of the painting while the former provides the fingerprint of the main chemical elements present in almost all layers (tens of microns) of the sample. The synergetic application of XRF and FORS is a key turn for non-invasive scientific analysis of works of art since it exhaustively describes the pigments employed by the masters and supplies a first insight into their distribution on the panels. In this scenario, Optical Microscopy (OM) applied directly on the painting surface, without any type of sampling, is traditionally deemed as a useful and descriptive tool for showing microscopic features such as craquelure brushstrokes or painting material distribution. It can be eventually expendable as a qualitative help during the discussion of spectroscopic data, but not considered fundamental. Nonetheless, the application of image processing protocols can make OM a concrete support for the characterization of paintings. In this work a new image analysis strategy has been introduced, its potential has been demonstrated studying different flesh tones from the panel "The Holy Family with St. Anne and the young St. John" by Bernardino Luini (Pinacoteca Ambrosiana Collection of Milan) and, finally, it has been discussed how OM could

quantitatively complete XRF and FORS analysis. The results show that optical microscopy, other than provide a glance of the investigated surface spots, effectively integrates the description given by the spectroscopic techniques and, properly managed, can be a useful resource for solving ambiguous cases.

Keywords: Pigments, XRF, FORS, Optical Microscopy, HSV model, Multivariate representation

1 Introduction

Bernardino Luini belongs to that circle of painters grouped as Leonardeschi [1]. Although there is no evidence that they met each other, Luini was so deeply charmed by Leonardo that he embodied his style (the so called Leonardismo) and played a key role in its great diffusion, mostly after his possible contact with some of the master's cartoons. The painting "The Holy Family with St. Anne and the young St. John (Sacra Famiglia con sant'Anna e san Giovannino)", an oil on wood held by the Pinacoteca Ambrosiana in Milan (panel A in figure 1), is inspired to the preparatory cartoon "The Virgin and the Child with St. Anne and St. John the Baptist" (No. 6337) created by Leonardo Da Vinci [2] held by the National Gallery in London. These considerations make the interest around the panel twofold: on one hand it sheds light on the author himself, on the other it describes the way Luini reinterpreted Leonardo; together they justify the effort for a complete campaign of studies. Elemental analysis is a key feature for the characterization of paintings; understanding the composition and the organization of materials on the works of art's layers discloses not only the creative process of the masters but also what concerns the workshops. The choice of raw materials, the techniques employed for both preparation and painting layers and the possible presence of co-workers and/or relationships with other ateliers help experts to unveil the history of the items and to design the best strategies for their conservation and/or restoration. Multidisciplinary non-invasive approaches for elemental analysis have been designed since some decades [3] [4] [5] but, in the last years, their spread is experiencing a new boost thanks to the introduction of portable, high performance instruments [6] [7] [8]. Focusing on the pigments employed by the artists, it is straightforward to recognize that the synergic use of X-Ray Fluorescence (XRF) and Reflectance Spectroscopy carried out by Fibre Optics (FORS) or not (like vis-RS) takes up a primary role. The first directly detects the presence of elements with $Z > 16$ [9] constituting the pigments, the latter guarantees a molecular and/or structural description of superficial layers, including organic-based pigments like lakes and pigments containing light elements, as ultramarine blue, that XRF cannot detect [10]. Together, they usually provide a wide description of the artist's palette [11] and often support more challenging task as parts of multiband spectral studies [12] or induce further non-invasive spectroscopic analyses, like FTIR and

Raman, or micro-invasive exams [13]. In this scenario, Optical Microscopy (OM) usually plays a marginal role and the images are often collected only to visualize the investigated areas. This practically reduces OM to an optional tool useful for documentary purpose (i.e. it shows where the spectroscopic data have been acquired) or, more rarely, expendable as qualitative help during the discussion of other kinds of data [14]. However, optical images contain large amounts of information that can be unveiled by means of proper methods. In this work, it has been introduced an original image analysis strategy aimed to give a quantitative foundation to the qualitative visual perception that the human eye gathers from the colours of paintings. The strategy has been applied to the study of different flesh tones from the "The Holy Family with St. Anne and the young St. John" and, with the support of multivariate data representation [15], it has been discussed how optical microscopy could effectively integrate the data acquired by XRF and/or FORS and to what extent OM could be a key resource for clarifying entangled situations. The obtained results support the idea that optical microscopy should no longer be considered a simple sight of the investigated surface but rather a source of quantitative information.

2 Materials and methods

2.1 Data detection

The experimental data have been collected with a multidisciplinary approach in different flesh tones areas distributed on the surface of the panel "The Holy Family with St. Anne and the young St. John". The considered areas (blue numbers in panel A of figure 1) have been chosen together with curators and, for each selected point, XRF and FORS spectra as well as an optical image have been collected.

2.1.1 Portable X-Ray Fluorescence (XRF)

The Bruker Artax 200 portable XRF spectrometer has been used: the instrument is equipped with Mo anode X-ray tube with a beam collimated at 0.65 mm in diameter (sample area excited 0.33 mm^2) and SSD detector. The principle of optical triangulation is applied for the adjustment of the working distance between the sample and the measuring head. The excitation beam and the optical axis of the detector meet at the measuring point when the laser spot matches cross hairs reported on the service CCD camera of the system; this procedure guarantees the reproducibility of the experimental conditions. The system presents an exchangeable filter slide with three positions and its sensitivity ranges from 2 to 40 keV. In the present work, the Mo filter (12.5 μm thick) has been used, the tube voltage and the anode current of the tube have been fixed respectively to 35 kV and 800 μA, the acquisition time has been 60 s while the acquisition energy range 2-25 keV. In the proposed data

analysis protocol, it has been considered the energy range between 3.2 and 14.5 keV in order to keep out the scattering peaks.

2.1.2 Fibre Optics Reflectance Spectroscopy (FORS)

The FORS spectra have been acquired with a portable visible-near infrared spectrophotometer HR4000 by Ocean Optics. The instrument was connected to a tungsten halogen light source (HL2000, Ocean Optics) and the radiation was transmitted through a quartz fibre optics bundle 1.5-meter-long, composed by six fibres to collect reflected light around the single central illuminating fibre using 45° x 45° measuring geometry. The spectrometer was simultaneously connected to a laptop and calibrated using white and black reflectance standards (Spectralon® 99% and a dark trap). For each spot, the reflectance spectra from 380 nm to 1000 nm have been acquired with a spectral resolution of 2.7 nm. However, the protocol has been applied to spectra in the wavelength range between 400 and 800 nm because the considered spectroscopic data don't bring useful information above the 800 nm and because for $\lambda < 400$ nm and $\lambda > 800$ the spectra are affected by high levels of noise.

2.1.3 Optical microscopy (OM)

The optical microscopy images have been detected employing a Dino-Lite polarized microscope that allows optical magnifications in the range 50x-230x. 230x magnification was preferred to better visualize pigment grains. Polarization is needed to reduce reflections due to the protective varnish. White LED lights grant proper illumination to the observed area. The output of the instrument is constituted by 8-bit 2400 x 1600 pixels RGB pictures detected in wide field reflection geometry within the visible range of the electromagnetic spectrum. Such images are 3D-matrices, their pixels are univocally defined by three number which represent the coordinates of a point in the colour space of Red, Green and Blue (RGB): the so-called *colour-cube*. Even if at unlimited resolution all the hues would appears as grains of different size, at the maximum resolution guaranteed by the Dino Lite, the OM pictures appear as constituted by a huge number of speckles of different colours and sizes over an almost uniform tint (panel B in figure 1). Therefore, discussing the OM data, the groups of pixels forming the speckles and those belonging to the layer that embeds the speckles have been called respectively inclusions/grains and basic gradation/basic tone

3 Data Handling

The key idea is to link the features arising from XRF, FORS and OM data for exploring if these techniques present mutual relationships and evaluating if their combined results can improve the description of the analysed points. Due to the similarity of the basic gradation of the flesh tones and due to the heterogeneity of the results to be combined, the classification cannot be accomplished by

simply listing the principal features of the single spots individually. It is necessary to explore the complexity of the whole dataset and to find out a group of significant parameters, called *descriptors* in the following of the paper, for each technique in order to emphasize differences and similarities between the flesh tones. If the XRF and FORS data can be directly processed for identifying the useful descriptors (see the related section), the handling of the optical microscopy pictures is complex and, due to the non-uniformity of the images, requires a multi-steps procedure, deeply described below. First, it is necessary to assemble the RGB pixels following a distinction criterion (segmentation), then the information contained into the clusters has to be represented into a colour space able to describe quantitatively the features of the images (modelling) and, only then, the best proper descriptors could be extrapolated.

3.1 OM Data Segmentation

In the image analysis, the first task to be solved is how to distinguish between the Foreground (FG, i.e. the interesting pixels of the picture) and the Background (BG, i.e. the remaining pixels). In the present paper, the answer to be fulfilled is complex because, even if all the spotted points belong to the group of the flesh tones, they can differ both for the basic gradation and for the inclusions (panel B in figure 1). The FG and BG cannot be uniquely defined within the dataset (for instance, compare sf-14 and sf-33 in panel B of figure 1) nor within the single image (see sf-25 in panel B of figure 1). Moreover, the distinction between foreground and background is purely formal because it is not possible to a priori assign more relevance to the basic tones rather than to the pigment grains when characterizing a painting surface layer. Finally, a hue classified as BG in an image can become FG into another (at glance white pixels could be considered BG in sf-25 but they could be assigned to FG in sf-33), especially if the data set spans over a wide range of similar tones. The home-made (MATLAB and Statistics Toolbox Release 2012b, The MathWorks, Inc., Natick, Massachusetts, United States) proposed data handling method has been designed for accounting the heterogeneities of the images, disregarding the hue of the basic gradation and of the inclusions. It is divided into two main steps:

- (i) the RGB to grey-scale conversion with the construction of what can be called Grey-Level-Image, GLI, (rows A and B in panel A of figure 2);

- (ii) the generation of the foreground/background masks (rows C, D and E in panel A of figure 2).

Deep in details, once the whole dataset has been transformed into a unique RGB matrix (step i), the range of the colour-cube's components have been equalized between 0 and 255 and, successively, the depth of the three components has been reduced from 8 to 4-bits (row A in panel A of figure 2 shows the re-binned 4-bit image of sf-04). These choices guarantee the entire dynamical range of the 8-bits

data to be used and, at the same time, the number of possible hues to be more easily handled with respect to that of the original images (it diminishes from $3*2^8$ to $3*2^4$). Due to the heterogeneity of the dataset, in the specific case of pigments grain distribution, it does not exist a convenient spatial feature for transforming the re-binned into grey-scale images; therefore the GLIs (row B in panel A of figure 2) have been generated basing on the frequencies of the RGB triplets. The pixel grey tones of the grey level images are due to the frequencies of the RGB triplet in the re-binned images: the lowest grey-tone is assigned to the pixels characterized by the more detected RGB triplet and so on. Therefore, the brightness of the grey tones is inversely proportional to the times a hue appears in the re-binned image, independently from the original colour. This implies two main outcomes:

- (i) the algorithm does not depend on the chromaticity of the images;

- (ii) the generation of the FG/BG masks can be accomplished by standard segmentation algorithms. In the second step of the data handling method, the masks (row C in panel A of figure 2) have been obtained basing on the iso-data algorithm [16]. The procedure splits the GLIs' pixels in foreground and background using an arbitrary grey-tone as starting threshold, it computes the means over the elements assigned to FG and BG and sets a new threshold to the average resulting from the FG and BG means; this operation is iterated till the threshold does not change any more. Row D in panel A of figure 2 shows the superimposition of the pixels' clusters obtained by the iso-data algorithm (the green Regions Of Interest, ROIs, are the perimeters surrounding the white areas of the mask in row C) on the original image: the ROIs divide the pixels of the original picture into the FG and BG masked images (row E in panel A of figure 2). Usually, the background is considered as the non-significant portion of the image but, since the present ROIs substantially surround the grains merged in the basic tone (see row D in panel A of figure 2), it would be better to speak about basic gradation's and inclusions' masks and realize that they both could have comparable relevance for the chromaticity of the painting. Due to the complexity of data analysis, the attention was focused on what has been formally mentioned as background; i.e. the basic gradations of the flesh tones (panel B in figure 2).

3.2 OM Data Modelling

Introduced by Alvy Ray Smith [17] the *hexcone* model translates the three dimensions of the colour-cube into a set of coordinates, called Hue, Saturation and Value (HSV), simulating the way an artist mixes paints on his palette. The painter first choses a pigment, then he softens or darkens the tint adding some black and white mixture until he gets the desired hue [17]. The coordinate H identifies the true colour (i.e. red, yellow, green, cyan, blue, magenta, etc); S quantifies how much the true colour has been diluted by white: a high S means deep colour while a low S (de-Saturation) identifies greyish tones (high whiteness); V is related to the brightness of the true colour and accounts for the

distance of the tint from black: the minimum and maximum V values correspond respectively to black and white because they respectively indicate the absence or the presence of chromaticity [18]. The hexcone model is constituted by N hexagonal disks (i.e. N hexagons and their interior) obtained projecting the colour-cube onto N planes perpendicular to the RGB space's grey axis (i.e. the colour-cube main diagonal). N is usually fixed equal to the depth of the RGB components (i.e. N = 256 for an 8-bit RGB colour image) in order to span from black, (R, G, B) = (0, 0, 0), to white (R, G, B) = (N-1, N-1, N-1), passing through the desired number of grey shades. Practically speaking, the HSV model is a non-linear geometrical transformation that, once normalized the RGB components in the range [0, 1], maps the colour-cube 3D Cartesian space into the hexcone cylindrical space as follow [17]:

$$H = \frac{1}{6}\begin{cases} 5 + b & \text{if} & R' = V & \text{and} & G' = X \\ 1 - g & \text{if} & R' = V & \text{and} & B' = X \\ 1 + r & \text{if} & G' = V & \text{and} & B' = X \\ 3 - b & \text{if} & G' = V & \text{and} & R' = X \\ 3 + g & \text{if} & G' = V & \text{and} & R' = X \\ 5 - r & \text{if} & G' = V & \text{and} & G' = X \end{cases}$$

$$S = \frac{V - X}{V}$$

$$V = \max(R', G', B')$$

with:

$$(R', G', B') = \frac{(R, G, B)}{N}$$

$$X = \min(R', G', B')$$

and

$$r = \frac{V - R'}{V - X}, \ g = \frac{V - G'}{V - X}, \ b = \frac{V - B'}{V - X}$$

H spans the colours from red to violet starting at 0° in counter-clockwise, S increases with the shades of the tones from the centre to the surface of the hexagonal disks, while V accounts for the tones increasing in the bottom-up direction within the hexcone. The way the HSV model has been designed implies that:

- (i) HSV is more closely related to the human eye perception than the RGB one (see for example [19] or [20]);

- (ii) differently from the other colour spaces, the hexcone presents at least one plane (i.e. an hexagonal disk) containing all the pure hues (i.e. S = 1) making the HSV particularly suitable when the same weight should be ascribed to different tints [17].

These characteristics clearly make the HSV model an ideal candidate for describing FG/BG image sets deriving from the OM data.

3.3 OM Descriptors

Once the home-made segmentation algorithm (MATLAB and Statistics Toolbox Release 2012b, The MathWorks, Inc., Natick, Massachusetts, United States) has automatically split the pictures into FGs and BGs, each background mask has been applied to the corresponding original RGB image and the resulting RGB masked images (panel B in figure 2) have been transformed into the hexcone space and used for finding the proper descriptors for OM as illustrated by supplementary figure 1 with the help of a sample image, I (panel A in supplementary figure 1). The HSV histogram of I (panel B in supplementary figure 1) is changed into a vector, indicated as $\vec{U}$. To construct $\vec{U}$, the frequencies of the (h, s, v) triplets, [f_{hsv}], have been considered as the elements of a 3D matrix, F (panels C in supplementary figure 1); each slice h (with h = 1, …, h, …, H) of F (panel C-1 in supplementary figure 1) constitutes a 2D sub-matrix, F_h, depicting the frequencies, [f_{hsv}], of the shades of a hue h (panel C-2 in supplementary figure 1). Following the row/column indexing, the elements of the F_h sub-matrices are organized into vectors of length S*V (panel C-2 in supplementary figure 1) that placed side by side constitute $\vec{U}$, a vector of length n = H*S*V, which represents linearly the HSV histogram of I (panel C-3 in supplementary figure 1). The maxima of $\vec{U}$ indicate the elements of the vector corresponding to the significant gradations, d_i, for the picture I (panel C-4 in supplementary figure 1 displays d_{1-5} for I), while the cumulative sum of $\vec{U}$ can be used for calculating the normalized cumulative distribution function (nCDF) of I (panel C-5 in supplementary figure 1) as follow:

$$CDF(k) = \sum_1^k U(k) \quad with \quad k = 1, \ldots\ldots\ldots, n$$

$$nCDF = \|CDF\|$$

Since the growth of the nCDF describes how the pixels collocate within the hexacone model (i.e. how they fill the colour space) and since the main steps of nCDF correspond to the maxima of $\vec{U}$ (i.e. the significant hues), evaluating the nCDF at the positions of the maxima, d_i, provides a mathematical description of I based on the HSV colour space. The iteration of this procedure for all the M masked

images of the dataset gives M sets of d_i, d_{i_m}, that put together provide the descriptors $D_j = \bigcup_{m=1}^{M} d_{i_m}$ for the OM's images. In this case study, the M = 13 HSV histograms related to the detection areas have been obtained adapting the work by Li Gong (MATLAB and Statistics Toolbox Release 2012b, The MathWorks, Inc., Natick, Massachusetts, United States) with H = 20, S = 8 and V = 4 for clustering the pixels into the bins of the histograms; the dimension of D_{j_1} results to be of 88 different indices. The setting of the HSV values have been experimentally chosen by the authors basing on the OM images acquired. Since the hexacone model translates the colour-cube into the digital representation which best mimic the human perception [17], the bins characterizing the HSV histograms can be considered as obtained following the same discriminators instinctively adopted by the eye (i.e. the hues and their gradations) with the crucial advantage that, being the HSV and RGB spaces connected by a geometrical transformation, they keeps the quantitative attribute proper of the digital images.

3.4 XRF and FORS Descriptors

For what concerns X-ray fluorescence analysis, the choice of the descriptors is quite easy. The XRF peaks in the spectra directly reflect the principal chemical elements present in the sample and the intensities of the peaks are related to the effective amounts (peak intensity and concentration are not directly proportional due to auto-absorption effects) of the elements with $Z > 16$ [9]. A home-made algorithm (MATLAB and Statistics Toolbox Release 2012b, The MathWorks, Inc., Natick, Massachusetts, United States) identifies the main chemical elements of the whole X-ray fluorescence dataset (panel A in supplementary figure 2). This is accomplished searching the sum of all the XRF spectra (panel B and inset of panel B in supplementary figure 2) for the main peaks. Therefore, the signals integrated around the energies of the peaks can be used for describing the acquired XRF data where the integration interval around each peak equals the first σ of a gaussian (orange horizontal lines in panel B and in the inset of panel B in supplementary figure 2) fitted to the relative maximum. The energies of the peaks (blue triangles in panel B and in the inset of panel B in supplementary figure 2) identify the descriptors for the XRF dataset. Even if the describing quantities are the integrated energies around the peaks, for the sake of brevity, the XRF descriptors have been sometimes referred using the energies of the peaks, E_{j_2} (Table 1). Searching for the descriptors of the FORS spectra (panel C in supplementary figure 2) is more complex because of the pigments' materials used to create flesh tones themselves and the nature of spectra not showing well defined peak, but larger bands and shoulders. Beside the fact that the pigments of the areas chosen do not show significant reflection/absorption bands in the visible range spectrum (400 – 800 nm), the

features commonly used for the classification of the spectra (i.e. maxima/minima and inflections [21]) cannot be expected to be distinctive of the data, also because spectra belong to very similar shades of colour. However, panel C in supplementary figure 2 reveals that, beyond a main common trend, some differences exist within the FORS spectra. This assumption can be verified looking at the change of concavity displayed by the spectra between 500 and 600 nm. It is evident that each flesh tone, typically based on different mixtures of lead white with S-shaped pigments like iron oxides (yellow or brown earths, ochre), vermillion, red lake, shows in this case an inflection in a narrow range around 575 nm [10] but, at the same time, the change of concavity takes place in different ways; therefore, if on the one hand the position of the flex does not fix a difference in reflectance curves, on the other, the slope of the spectrum at the flex does. Panel D in supplementary figure 2 illustrates this clue comparing the spectra from sf-13 and sf-33: they both present an inflection at $\lambda = 580$ nm but, at the same time, the tangents to the curves form different angles at the horizontal axis (respectively 54° and 66°). Table 2 lists the 19 wavelengths, λ_{j_3}, that corresponds to a peculiarity (not necessary an inflection) of at least one FORS profile and thus the slopes of the spectra at λ_{j_3} have been identified as the descriptors for the reflectance spectroscopy dataset. Even if the descripting parameters are the slope of the spectra at λ_{j_3}, for sake of simplicity, the FORS descriptors have been sometimes referred simply by their related wavelengths, λ_{j_3}. The fact that the number of descriptors for XRF and FORS corresponds is purely coincidental.

4 Data Representation (Multivariate Display Mode)

As the amount of data increases both in terms of variety as well as complexity (multidimensional data), the well-known display modes (scatter plot, histograms, maps and so on) lose effectiveness since they are not suitable for representing multidimensional datasets [22]; luckily, the problem can be circumvented using the so-called graphic display methods [23]. Glyphs, introduced by Anderson in 1957 [24], are one of the most widely spread graphic display mode; they constitute an important medium for exploratory analysis because they evoke underlined relationships that might not be promptly detected with mathematical approaches [23]. A glyph-plot corresponds to a single studied object, m, within a dataset (in this case: the OM, XRF or FORS dataset) of dimension M. The m-th object is depicted as a "star" with j spoke whose j-th spoke, S_{j_m}, refers to the j-th parameter selected for describing the dataset (i.e. the j-th descriptor of the related dataset) and is proportional in length to the value that the j-th parameter assumes within the j-th parameters of the whole dataset normalized in the range [0, 1] (panel A in figure 3). The Glyphs plots have been chosen for data representation because the analyses of OM, XRF and FORS data in terms of descriptors all return more than three

parameters. Moreover, employing glyphs as markers in standard plot, the user can immediately perform a comparison between the different data types. The glyph plots related to OM, XRF and FORS data are characterized respectively by 88, 19 and 19 spokes.

5 Results and Discussion

The experimental results about the painting "The Holy Family with St. Anne and the young St. John" confirm that Luini, as expected for a pupil or follower of Leonardo da Vinci, used the typical palette of his period [25]. In particular, to render the gradation of the flesh tones in his paintings, he mixed and layered lead white with vermillion, ochres and lakes in different mixture and proportion, depending on the desired chromatic effect [26]. In facts, the XRF analysis (panels A and B in supplementary figure 2 and table 1) always identifies K (k_α at 3.3 keV), Fe (k_α and k_β respectively at 6.4 and 7.1 keV) peculiar of ochres. The low amounts of Cu (k_α at 8 keV) suggest the presence of a few grains of copper-based pigments like verdigris, presumably in the underlayers. Ca (k_α and k_β respectively at 3.7 and 4 keV) and Sr (k_α at 14.1 keV) that can be mainly related to the preparation layer of the panel; Hg (L_α and L_β respectively at 10 and 11.8 keV) uniquely identifying the vermilion and Pb (L_α, L_β, L_l and L_η respectively at 10.5, 12.6, 9.2 and 11.3 keV), which is the characterising element of the lead white, lead-based yellows and minium (orange lead oxide), the latter not found in the examined points. The FORS spectra (panels C and D in supplementary figure 2) show in almost all the analysed areas the typical behaviour of the vermillion pigment, with a sharp growth around 575 nm and no relevant reflection/absorption maxima within 400 and 800 nm. Only for sf-29 and sf-66, peculiar spectra have been detected within the acquired dataset: the first is similar to a yellow ochre, the second assumes a singular behaviour above 600 nm reminding the presence of a coccid-derived red lake, like kermes. Beyond this analytical information, the direct observations of OM images show that there exists a complex scenario of relationships within the considered flesh tones (panel B in figure 1): along white pigments (lead white), different red/pink grains (vermillion and sometimes red lake) can be observed, as well as brown (ochre or earth), black (carbon black) ones. Some quite large green inclusions can also be noticed, their morphology and colour are more likely associated to a green earth than to copper-based pigments. The complexity is evident even limiting the attention to the basic gradation of the pigments (panel B in figure 2). Spots sf-04, sf-06, sf-20 and sf-23 display yellow shades while the triplet sf-29, sf-55 and sf-66 basic colours turn toward pink tonalities. Points sf-13, sf-14 and sf-33 distinguish themselves for their singularity while the other ones (i.e. sf-11, sf-25 and sf-30) remain pending since they appear to mix the peculiarities of groups and stand-alone spots. The analysis of the HSV descriptors has been designed for investigating if

these qualitative considerations can be translated into quantitative information and the glyph plots have been identified as an effective tool for illustrating the obtained results. Panel B in Figure 2 and panel B in figure 3 allow to compare the model with the subjective perceptions: besides the confirmation of the main groups qualitatively highlighted (refer to the colours of the codes in panel B of figure 2), the glyph plots suggest a classification for the remaining spots. sf-30 presents a dark brown halo superimposed to a yellowish basic gradation, and its glyph resembles the properties of both sf-13 and the group formed by sf-04, sf-06, sf-20 and sf-23, i.e. respectively the browner point and the pigments mainly affected by yellow shades. Glyph of sf-25 results very similar to the pinkish triplet sf-29 – sf-55 – sf-66 even if the brown trace could recall sf-13 and sf-30. Finally, sf-11 appears to be more compatible with the yellowish points rather than the pinkish triplet. The indications given by the OM images could not completely match those given by X-ray fluorescence and/or reflectance spectroscopy analysis. Starting from the consideration that data sets belong to a painting which shows different pictorial layers and peculiar painting practices, the employed analytical techniques have been chosen to get synergic and complementary information. They took advantage of the different penetration depths of electromagnetic radiation in different wavelength ranges. In general, penetration depth depends on the incident and the outgoing radiation wavelength as well as on the material investigated. Namely for visible and IR radiation, the penetration depth is linked to the refractive index and the absorption of different materials present in the pictorial layers, ranging from a few microns up to one or two hundred microns under the surface. On the contrary, X-rays can penetrate deep into the matter: in this specific case, incident X radiation can surely pass through the complete stratigraphy. Outgoing characteristic X fluorescence of medium-heavy elements can still pass the whole thickness, while relatively light elements (such as Ca and K) have a higher probability to be absorbed. Therefore, the information given by these three very different techniques are surely complementary, but not always correlated. Moreover, it has to be noticed that while the analysis of the OM images can be split into foreground and background, XRF and FORS always refer to the whole analysed areas; therefore, it is expectable that the OM descriptors of the foreground masked images could be different from the background ones. Indeed, they could be differently related to the descriptors of the spectroscopic analyses.

As expected on the base of the previous considerations, the glyph representations of XRF (panel C in figure 3) and FORS (panel D in figure 3) at their respective descriptors depict different scenarios with respect to that given by OM (panel B in figure 3). Surely, until a connection between the colour space and the spectroscopic dimension would not be established, all the considerations could be given as the results of the three techniques that keep equal reliability and the colour analysis add only few significant details. The observation of the co-occurrence elemental plots hints an interesting point of

view. Figure 4 shows the HSV descriptors' glyphs organized in terms of some chemical elements identified by XRF. In panels A-1 (3.3 vs 10.5 keV) and A-2 (10 vs 10.5 keV) the pigments result ordered in a manner similar to that suggested by the subjective observations of the BG masked images (panel B in figure 2) and by the multivariate representation of the pictures (panel B in figure 3); the singularities, the groups and the assignation of uncertain points can be re-found with the exception of sf-25 which results unrelated with respect to the pinkish triplet. The arrangement of the flesh tones is further emphasized by the 3D co-occurrence plot (panel A-3 in figure 4); where the yellowish pigments appear more selectively clustered into two couples (sf-04 – sf-06 and sf-20 – sf-23), the singularities are clearly spread at the edges of the graph with sf-30 and sf-25 (the spots that show a brown halo) as the nearest to sf-13 and the members of the pinkish triplet which keep relatively close each other. Moreover, no other co-occurrence plot based on the other main chemical elements identified by XRF (data not shown) generates a distribution of the pigments substantially coherent with the HSV multivariate representation; therefore, besides the expected effectiveness of the hexcone model for quantifying the subjective perception, the present case seems to disclose a specific role for some of the elements identified by XRF. It is possible to speculate that the basic gradation of these flesh-tones is to be ascribable to Pb, Hg and K; iron is present everywhere, in all nuance ochre (red, yellow or burnt). For copper, this could indicate the effective presence in lower layers, such as coloured priming, that do not affect the hues of the outer layer. These considerations are consistent with the hypothesis that to render the flesh tones, the author mixed and layered lead white with vermillion, and that he used earth and ochres, sometimes a red lake, to give different hues. Moreover, the fact that Ca dependent plots do not add significant information is consistent with what expected for an element present only in the preparation layer of the panel rather than in the painting layers. The distribution of the OM glyphs observed in panel A-3 of figure 4 is in good agreement with that obtained referring to the descriptors of the FORS spectra (panel B in figure 4). The data distribution shows that, except for sf-66 (depicted by the inset of panel B in figure 4), the mutual relationships unveiled by the 3D elemental graph can be recovered organizing the investigated points on the base of the slopes of the reflectance spectra at three particular wavelengths within the descriptors of the FORS data: 422, 571 and 716 nm. Besides the fact that they are equally spaced, the wavelengths of panel B in figure 4 are particularly interesting because they match perfectly the features of the main coloured pigment used by Luini for the flesh tones: the vermilion which has a reflectance spectrum characterized by two flat regions (respectively below 500 nm and above 600 nm) and a sharp transition (near 575 nm) typical of the semiconductor behaviour of HgS [27]. Again, the singularities, the couples within the yellowish areas, the behaviour of sf-29 and sf-55 of the pinkish triplet and even the odd collocation of sf-25 can be identified within the slope co-occurrence plot.

6 Conclusion

The proposed image processing protocol supports the well-established fact that the basic pigment used by Luini for the flesh tones of his paintings was the vermillion [1]. Besides this comfortable confirmation, the intriguing suggestion is that, in the case of the basic gradations (panel B in figure 2) of the studied flesh tones of the "The Holy Family with St. Anne and the young St. John", the features that spectroscopically identify the vermillion arise as the key turn for unveiling an un-expected and non-purely coincidental relationship between spectroscopy and optical microscopy data. The XRF descriptors linked to the vermillion mixed with lead white (i.e. the integrated energies around the Hg and Pb peaks) give rise to a distribution of the areas (panel A in figure 4) compliant with the classification suggested by the HSV multivariate representation (panel B in figure 3). Moreover, the deductions obtained by the comparison between XRF and OM find good confirmation in the analysis of the relationships between OM and FORS. The combination of the three particular descriptors of the FORS dataset used in panel B of figure 4 not only gives an arrangement similar to that suggested by the HSV multivariate representation (panel B in figure 3) but also confirms the relevance of the features of the vermillion as peculiar in the relationships between the microscopy and spectroscopy for the basic gradation of the flesh tones. Indeed, the selected wavelengths identify the two flat regions ($\lambda < 500$ nm and $\lambda > 600$) and the transition ($\lambda \approx 575$ nm) of the vermillion.

On one hand the relationships highlighted by the proposed method cannot be considered to be perfect: the discussed anomalous behaviours of sf-25 and sf-66 within the OM-XRF/FORS comparisons, the current lack of a correspondence between XRF and FORS that would complete the interconnection between the three techniques, the relevance of K for the OM-XRF comparison remain un-answered questions and suggest that the method should be improved, especially if the future tasks would involve the analysis of the foreground masked images (i.e. the inclusions of the investigated areas). On the other hand, the results discussed in this paper shows that OM could be:

- (i) a support to XRF and FORS because it confirms the deduction of the main chemical elements and pigments constituting the flesh tones;

- (ii) an improvement of the data description given by the spectroscopic techniques because OM suggests a further classification of the flesh tones based on the elemental and/or structural features of the spectra;

- (iii) or even a partial alternative to FORS because the good agreement between OM multivariate and XRF elemental analysis suggests this couple as a valid alternative to the usual synergy XRF-FORS in the determination of the pigments.

Summarising, the proposed protocol for the first time concretely demonstrates that, besides the documental function, optical microscopy has a real potential for the characterization of paintings' surfaces. Finally, it is interesting to note that the high affinity between the HSV space analysis and the subjective perception supports the hypothesis that, at least for what concerns the colours of a painting, the glance impressions could be encoded by quantitative models.

Acknowledgments

Conflict of Interest (COI)

The authors declare that there is no conflict of interest.

CRediT

Anna Galli: Investigation, Conceptualization, Methodology, Writing - review & editing, Supervision

Michele Caccia Conceptualization, Validation, Formal analysis, Software, Writing - review & editing

Letizia Bonizzoni: Investigation, Validation

Marco Gargano: Investigation

Nicola Ludwig: Investigation

Gianluca Poldi Investigation

Marco Martini Supervision

References

[1]   G. Bora, D. A. Brown and M. Carminati, I leonardeschi: l'eredità di Leonardo in Lombardia, Skira-Berenice, 1998.

[2]   E. Harding, A. Braham, M. Wyld and A. Burnstock, "The restoration of the Leonardo cartoon," *National Gallery Technical Bulletin,* vol. 13, pp. 4-27, 1989.

[3]   P. Vandenabeele, B. Wehling, L. Moens, B. Dekeyzer, B. Cardon, A. Bohlen and R. Klockenkämper, "Pigment investigation of a late-medieval manuscript with total reflection X-ray fluorescence and micro-Raman spectroscopy," *Analyst,* vol. 124, pp. 169-172, 1999.

[4]   G. Bitossi, R. Giorgi, M. Mauro, B. Salvadori and L. Dei, "Spectroscopic techniques in cultural heritage conservation: a survey," *Applied Spectroscopy Reviews,* vol. 40, pp. 187-228, 2005.

[5]   P. Ricciardi, J. K. Delaney, L. Glinsman, M. Thoury, M. Facini and E. R. Rie, "Use of visible and infrared reflectance and luminescence imaging spectroscopy to study illuminated manuscripts: pigment identification and visualization of underdrawings," in *O3A: Optics for Arts, Architecture, and Archaeology II*, 2009.

[6]   G. Sciutto, P. Oliveri, S. Prati, M. Quaranta, S. Bersani and R. Mazzeo, "An advanced multivariate approach for processing X-ray fluorescence spectral and hyperspectral data from non-invasive in situ analyses on painted surfaces," *Analytica chimica acta,* vol. 752, pp. 30-38, 2012.

[7]   L. Bonizzoni, S. Bruni, A. Galli, M. Gargano, V. Guglielmi, N. Ludwig, L. Lodi and M. Martini, "Non-invasive in situ analytical techniques working in synergy: the application on graduals held in the Certosa di Pavia," *Microchemical journal,* vol. 126, pp. 172-180, 2016.

[8]   A.-C. Saint, V. Dritsa, E. Cheilakou, E. Valavani, C. Margariti, K. Efthimiou and M. Koui, "Non-invasive Identification of the Pigments and Their Application on Theophilos Hatzimihail's Easel Paintings," in *International Symposium on the Conservation of Monuments in the Mediterranean Basin*, 2017.

[9]   I. Liritzis and N. Zacharias, "Portable XRF of archaeological artifacts: current research, potentials and limitations," in *X-ray fluorescence spectrometry (XRF) in geoarchaeology*, Springer, 2011, pp. 109-142.

[10] J. K. Delaney, P. Ricciardi, L. D. Glinsman, M. Facini, M. Thoury, M. Palmer and E. R. d. l. Rie, "Use of imaging spectroscopy, fiber optic reflectance spectroscopy, and X-ray fluorescence to map and identify pigments in illuminated manuscripts," *Studies in Conservation,* vol. 59, pp. 91-101, 2014.

[11] K. Trentelman, M. Bouchard, M. Ganio, C. Namowicz, C. S. Patterson and M. Walton, "The examination of works of art using in situ XRF line and area scans," *X-Ray Spectrometry: An International Journal,* vol. 39, pp. 159-166, 2010.

[12] M. Gargano, A. Galli, L. Bonizzoni, R. Alberti, N. Aresi, M. Caccia, I. Castiglioni, M. Interlenghi, C. Salvatore, N. Ludwig and M. Martini, "The Giotto's workshop in the XXI century: looking inside the "God the Father with Angels" gable," *Journal of Cultural Heritage,* vol. 36, pp. 255-263, 2019.

[13] M. L. Amadori, G. Poldi, S. Barcelli, P. Baraldi, M. Berzioli, A. Casoli, S. Marras, G. Pojana and G. C. F. Villa, "Lorenzo Lotto's painting materials: an integrated diagnostic approach," *Spectrochimica Acta Part A: Molecular and Biomolecular Spectroscopy,* vol. 164, pp. 110-122, 2016.

[14] S. Bracci, O. Caruso, M. Galeotti, R. Iannaccone, D. Magrini, D. Picchi, D. Pinna and S. Porcinai, "Multidisciplinary approach for the study of an Egyptian coffin (late 22nd/early 25th dynasty): Combining imaging and spectroscopic techniques," *Spectrochimica Acta Part A: Molecular and Biomolecular Spectroscopy,* vol. 145, pp. 511-522, 2015.

[15] P. C. Saxena and K. Navaneetham, "Comparison of Chernoff-type face and non-graphical methods for clustering multivariate observations," *Computational statistics & data analysis,* vol. 15, pp. 63-79, 1993.

[16] T. W. Ridler and S. Calvard, "Picture thresholding using an iterative selection method," *IEEE transactions on Systems, Man and Cybernetics,* vol. 8, pp. 630-632, 1978.

[17] A. R. Smith, "Color gamut transform pairs," *ACM Siggraph Computer Graphics,* vol. 12, pp. 12-19, 1978.

[18] V. Chernov, J. Alander and V. Bochko, "Integer-based accurate conversion between RGB and HSV color spaces," *Computers & Electrical Engineering,* vol. 46, pp. 328-337, 2015.

[19] I. Nunez-Garcia, R. A. Lizarraga-Morales and G. Hernandez-Gomez, "Classification of Paintings by Artistic Genre Integrating Color and Texture Descriptors," in *Proceedings of the 2018 International Conference on Artificial Intelligence and Pattern Recognition*, 2018.

[20] N. A. Ibraheem, M. M. Hasan, R. Z. Khan and P. K. Mishra, "Understanding color models: a review," *ARPN Journal of science and technology,* vol. 2, pp. 265-275, 2012.

[21] M. Bacci, "UV-VIS-NIR, FT-IR, and FORS Spectroscopies," in *Modern analytical methods in Art and Archaeology*, New York-Chichester-Weinheim-Brisbane-Singapore-Toronto, 2000, pp. 321-360.

[22] J. R. Beniger and D. L. Robyn, "Quantitative graphics in statistics: A brief history," *The American Statistician,* vol. 32, pp. 1-11, 1978.

[23] D. L. Huff, V. Mahajan and W. C. Black, "Facial representation of multivariate data," *Journal of Marketing,* vol. 45, pp. 53-59, 1981.

[24] E. Anderson, "A semigraphical method for the analysis of complex problems," *Proceedings of the National Academy of Sciences of the United States of America,* vol. 43, p. 923, 1957.

[25] L. Bonizzoni, S. Caglio, A. Galli and G. Poldi, "Around and after Leonardo: The Painting Technique of a 'Virgin of The Rocks' attributed to Bernardino Luini," in *VII congresso nazionale di archeometria*, 2012.

[26] L. Bonizzoni, M. Gargano, N. Ludwig, M. Martini and A. Galli, "Looking for common fingerprints in Leonardo's pupils using nondestructive pigment characterization," *Applied spectroscopy,* vol. 71, pp. 1915-1926, 2017.

[27] A. Cosentino, "FORS spectral database of historical pigments in different binders," *53 TECHNICAL,* p. 54, 2014.
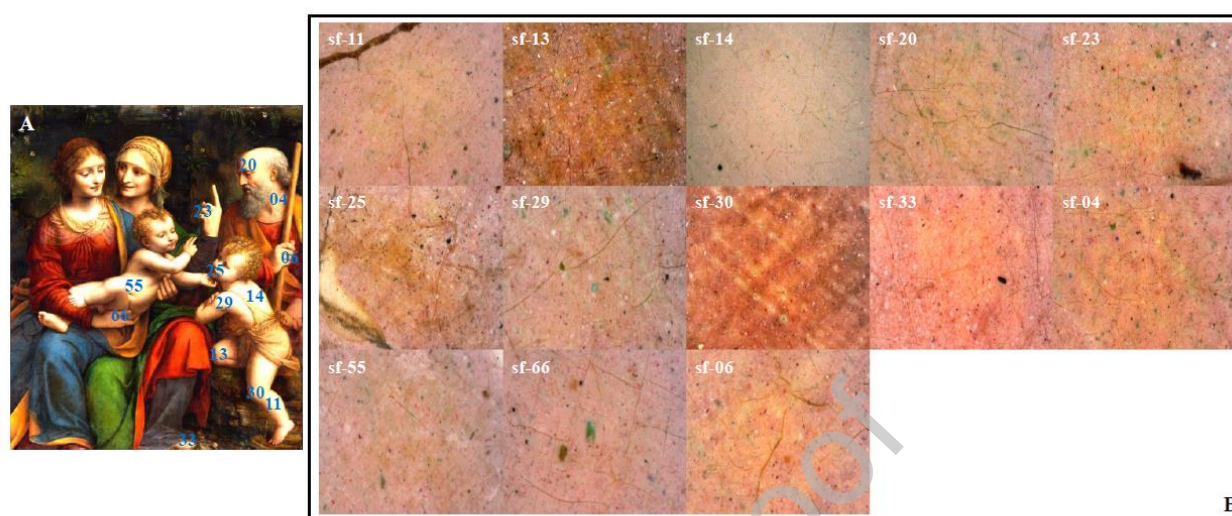
Captions

Figure 1: The painting "The Holy Family with St. Anne and the young St. John" by Bernardino Luini and the analysed areas. **Panel A**: the painting; the **blue numbers** indicate the areas where the experimental data have been acquired. **Panel B**: the RGB images collected by the Dino-Lite polarized microscope; the numbers of the **codes** (sf-number) superimposed to the pictures correspond to the areas highlighted in panel A by the blue numbers; the prefix "sf" recalls that the data have collected on the painting ("Holy Family = Sacra Famiglia" → "sf").
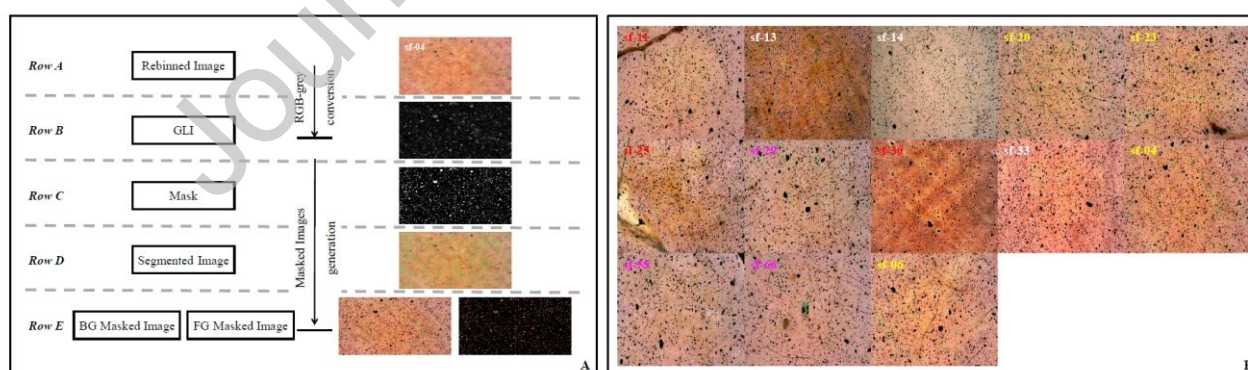

Figure 2, the algorithm that prepares the OM images for the colour analysis and the obtained BG masked images. **Panel A**, **left side**: the sketch of the algorithm used for evaluating the FG and BG masked images. **Panel A**, **right side**: the application of the algorithm to one of to the detected areas: sf-04; **row A**, the re-binned image, and **row B**, the GLI, illustrate the first part of the algorithm while **row C**, the mask, **row D**, the segmented image, and **row E**, the FG and BG masked images, describe

the main steps of the second part of the algorithm. **Panel B**: the optical microscopy BG masked images obtained by the application of the algorithm to the pictures of panel B in figure 1. The **colours** assigned to the codes refer to the subjective perception of the spotted areas discussed in the text; the yellow, pink, white and red codes refer respectively to the yellow shaded areas, the pinkish triplet, the singularities and the pending points.
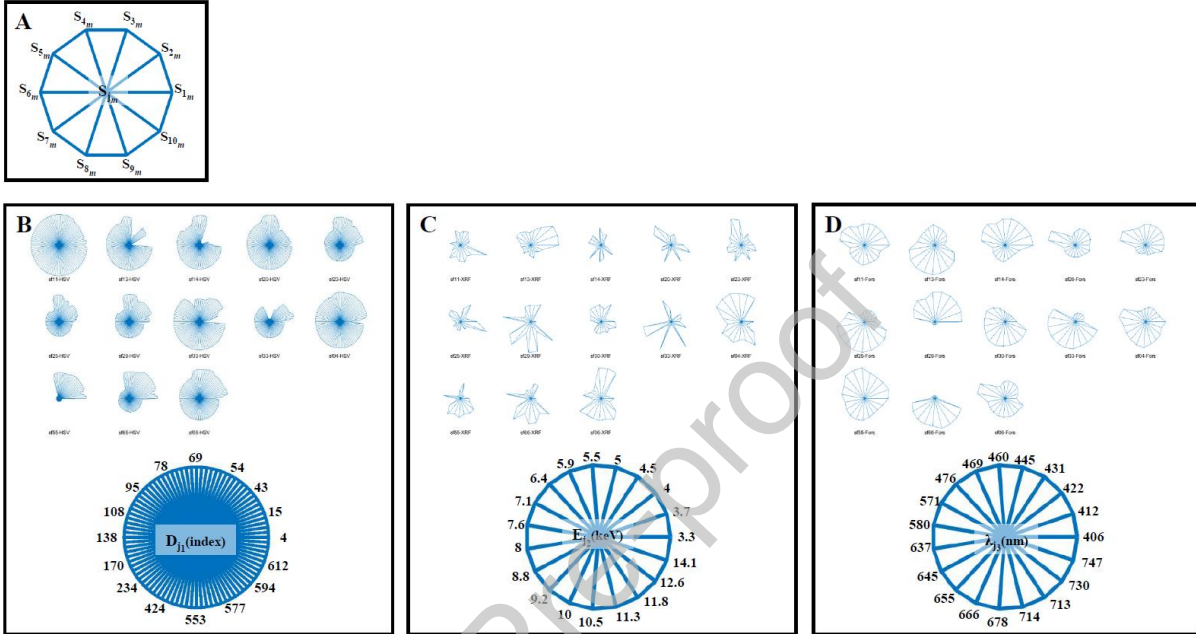

Figure 3: the multivariate data representation by glyph plots **Panel A**: the explanation of how to read a glyph plot referred to a generic m-th object of a dataset constituted by M objects with m = 1, ..., m, ..., M. The values assumed by the descriptors, S_{j_m}, are disposed along branches around a central point as the strokes of a star; usually S_{1_m} is disposed on the branch directed from the centre toward the right edge of the plot; the placement of the remaining descriptors continues starting from S_{1_m} in counter clock wise. The M values assumed by every j descriptor are normalized between 0 and 1. In the example of panel A the glyph is characterized by 10 descriptors which, for simplicity, have been fixed to the same value $S_{j_m} = 1$ for j = 1, ..., 10. **Panel B**, **C** and **D**: the glyph plots obtained by the OM, XRF and FORS datasets of the studied areas; the illustrative glyph plots in the lower parts of the panels shows how the descriptors D_{j_1}, E_{j_2} and λ_{j_3} take place along the branches. In panel B it was not possible to report all the values of D_{j_1} because of space opportunity; however, the reported values are enough to illustrate the fact that they are concentrated within the red, orange, yellow and violet slices of the HSV histogram as expected for a dataset constituted by the basic gradation of some flesh tones

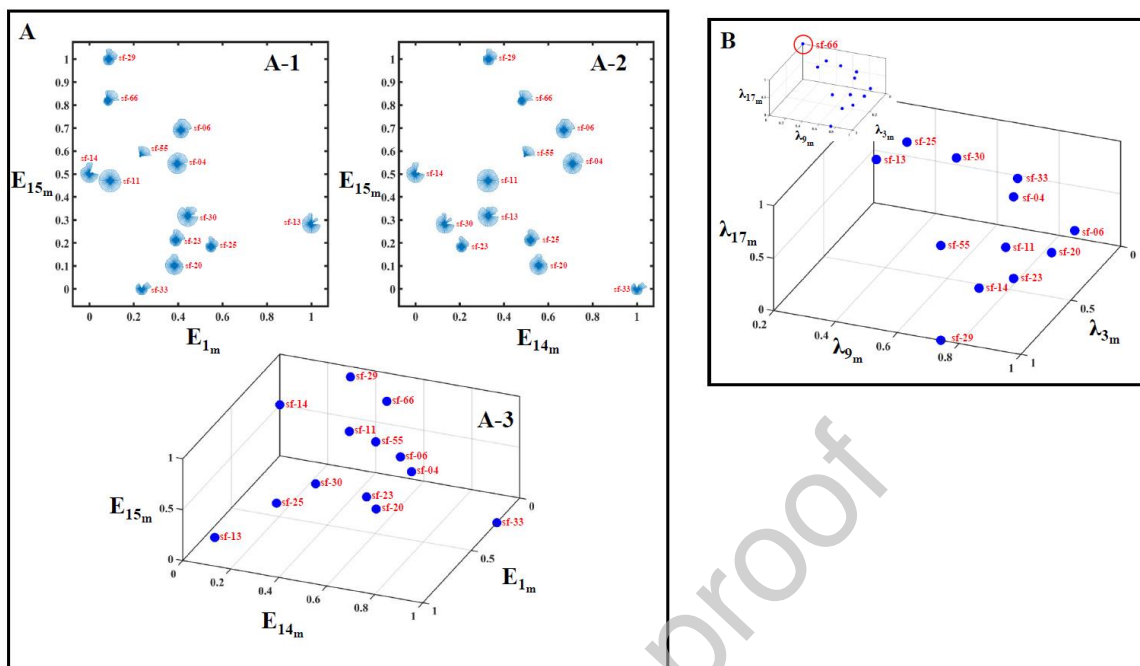(see panel B in supplementary figure 1 for check the colour localization of the slices within the HSV space).

Figure 4: the co-occurrence plots. **Panel A**: the most significant co-occurrence plots within all the possible combinations based on the E_{j_2} descriptors for the XRF dataset; the energies used in the sub-panel A-1, A-2 and A-3 are $E_{1_m} = 3.3$ keV, $E_{14_m} = 10$ keV and $E_{15_m} = 10.5$ keV. **Panel B**: the most significant 3D co-occurrence plot for the λ_{j_3} descriptors of the FORS dataset; the wavelengths used for both the panel and the inset are $\lambda_{3_m} = 422$ nm, $\lambda_{9_m} = 571$ nm and $\lambda_{17_m} = 716$ nm. **Panel B**, **inset**: the anomalous behaviour of the acquired area sf-66 within the FORS dataset.

Table 1: the list of the energies, E_{j_2}, used for indicating the descriptors for the XRF dataset; below every E_{j_2} the relative X-ray transitions have been reported

E(keV)	3.3	3.7	4	4.5	5	5.5	5.9	6.4	7.1	7.6
X-ray transition	k_α (K)	k_α (Ca)	k_β (Ca)	k_α (Ti)	k_β (Ti)	k_α (Cr)	k_β (Cr)	k_α Fe	k_β (Fe)	k_α (Co)
E(keV)	8	8.8	9.2	10	10.5	11.3	11.8	12.6	14.1	
X-ray transition	k_α (Cu)	k_β (Cu)	L_l (Pb)	L_α (Hg)	L_α (Pb)	L_η (Pb)	L_β (Hg)	L_β (Pb)	k_α (Sr)	

Table 2: the list of the wavelengths, λ_{j_3}, used for indicating the descriptors for the FORS dataset

λ(nm)	406	412	422	431	445	460	469	476	571	580
	637	645	655	666	678	714	716	730	747	